RESEARCH ARTICLE
SPACE PHYSICS: IONOSPHERIC PHYSICS

Earth and Planetary Physics
4: 571–578, 2020
doi: 10.26464/epp2020061

On the radar frequency dependence of polar mesosphere summer echoes

ShuCan Ge[1], HaiLong Li[1*], Lin Meng[1], MaoYan Wang[2], Tong Xu[3], Safi Ullah[1], Abdur Rauf[1], and Abdel Hannachid[4]

[1]School of Electronic Science and Engineering, University of Electronic Science and Technology of China, Chengdu 610054, China;

[2]School of Physics, University of Electronic Science and Technology of China, Chengdu 610054, China;

[3]National Key Laboratory of Electromagnetic Environment, China Research Institute of Radio Wave Propagation, Qingdao 266107, China;

[4]Department of Meteorology, Stockholm University, SE-106-91, Stockholm, Sweden

Key Points:

- The characteristics of polar mesosphere summer echoes (PMSEs) simultaneously observed by both very high frequency (VHF) and ultra high frequency (UHF) radars are presented
- High-frequency heating has a limited effect on the intensity of PMSEs when the UHF electron density is increased because of energetic particle precipitation
- The volume reflectivity has been further confirmed to be inversely proportional to the fourth power of radar frequency

Citation: Ge, S. C., Li, H. L., Meng, L., Wang, M. Y., Xu, T., Ullah, S., Rauf, A. and Abdel, H. (2020). On the radar frequency dependence of polar mesosphere summer echoes. *Earth Planet. Phys.*, *4*(6), 571–578. http://doi.org/10.26464/epp2020061

Abstract: Polar mesosphere summer echoes (PMSEs) are very strong radar echoes in the polar mesopause in local summer. Here we present the frequency dependence of the volume reflectivity and the effect of energetic particle precipitation on modulated PMSEs by using PMSEs observations carried out by European Incoherent SCATter (EISCAT) heating equipment simultaneously with very high frequency (VHF) radar and ultra high frequency (UHF) radar on 12 July 2007. According to the experimental observations, the PMSEs occurrence rate at VHF was much higher than that at UHF, and the altitude of the PMSEs maximum observed at VHF was higher than that at UHF. Overlapping regions were observed by VHF radar between high energetic particle precipitation and the PMSEs. In addition, high-frequency heating had a very limited impact on PMSEs when the UHF electron density was enhanced because of energetic particle precipitation. In addition, an updated qualitative method was used to study the relationship between volume reflectivity and frequency. The volume reflectivity was found to be inversely proportional to the fourth power of radar frequency. The theoretical and experimental results provide a definitive data foundation for further analysis and investigation of the physical mechanism of PMSEs.

Keywords: Polar mesosphere summer echoes; artificial electron heating; volume reflectivity; energetic particle precipitation

1. Introduction

Polar mesosphere summer echoes (PMSEs) are strong echoes detected by radar in the polar mesopause in local summer. Czechowsky et al. (1979) and Ecklund and Balsley (1981) first studied PMSEs by SOUSY (sounding system) and MST (mesosphere–stratosphere–troposphere) radar measurements, respectively. Since then, PMSEs have been studied in depth both theoretically and experimentally (Reid et al., 1988, 1989; Czechowsky et al., 1989; Rapp and Lübken, 2004).

Active heating experiments of PMSEs provide a new method of finding dusty plasma parameters in the mesosphere. Chilson et al. (2000) first presented the artificial electron heating effects on PMSEs by very high frequency (VHF) radar and found significant variations in the intensity of PMSEs during high-frequency (HF) heating. Later, La Hoz et al. (2006) observed a similar response of PMSEs to HF heating with ultra high frequency (UHF) radar. Havnes et al. (2003, 2007) used different heating sequences (such as heating for 20 s, closing for 160 s) for the heating experiments and found that the PMSEs overshoot event. That is, when the radio wave is turned on, PMSEs are immediately weakened or even disappear because the increase in electron temperature from radio wave heating causes the diffusion of ions and electrons. This disrupts the balance between dust charges and plasma densities; hence, PMSEs decrease by the reduction in electron density irregularities (La Hoz and Havnes, 2008). When the radio wave is turned off, the PMSEs rebound significantly and then slowly return to their preheated state. When decreasing the size of the dust radius, the dust charging time becomes greater than the plasma adjustment time, which produces the PMSEs overshoot event (Scales, 2004; Chen C and Scales, 2005). Much theoretical work has been done to explain this overshoot effect (Kassa et al., 2005; Mahmoudian et al., 2011; Senior et al., 2014; Blagoveshchenskaya

Correspondence to: H. L. Li, hailong703@163.com
Received 22 MAY 2020; Accepted 23 JUN 2020.
Accepted article online 07 AUG 2020.

et al., 2015; Havnes et al., 2015; Mishin et al., 2016; Wang et al., 2016).

Artificial electron heating experiments are known to be limited by many environmental factors, such as energetic particle precipitation (EPP). Energetic particle precipitation refers to highly energetic electrons, protons, neutrons, and ions that are accelerated into the atmosphere through various geomagnetic processes. They enter the atmosphere mainly in the geomagnetic polar regions and have a significant impact on the ionization, chemistry, temperature, and density of the mesosphere (Sinnhuber et al., 2012; Yi W et al., 2017a, b, 2018; Zou ZC et al., 2020). Some related reports (Zhang BC et al., 2001; Cai HT and Ma SY, 2007) have been presented but still no flawless study has been done on PMSEs heating experiments under the effect of EPP. The literature reveals that volume reflectivity shows an enormous frequency dependence (Cho and Kelley, 1993; Rapp and Lübken, 2004; Li HL et al., 2010). The relationship between the PMSEs volume reflectivity and radar frequency still lacks complete results. Hence, it is necessary to provide further details on the relationship between the PMSEs volume reflectivity and radar frequency. It is useful to elucidate the structural properties of the possible generation mechanism of strong radar echoes in the polar summer mesosphere region.

To study the validity of theoretical expectations, a common volume and simultaneous observations should ideally be used as tools. The aim of this research was to investigate the characteristics of PMSEs during artificial electron heating experiments in the VHF and UHF bands and to analyze the relationship between the PMSEs volume reflectivity and radar frequency under the influence of EPP.

Table 1. European Incoherent SCATter (EISCAT) radar parameters and experimental configuration.

Parameter	EISCAT VHF	EISCAT UHF
Geographic coordinates	69°35 N, 19°14 E	69°35 N, 19°14 E
Frequency (MHz)	224	930
Wavelength (m)	1.34	0.32
Altitude resolution (km)	0.3	0.45
Time resolution (s)	5	6
Beam width (°)	1.2 × 1.6	0.7
System temperature (K)	250–350	110
Radar program	arcdlayer	manda
Heating cycle	180 s (20 s on, 160 s off)	
Pump wave mode	Alternate O wave and X wave modes	
Pump wave frequency (MHz)	5.423	
Pump wave direction	Vertical	
Pump wave transmitter power (MW)	360	
Altitude range (km)	59.7–139.5	

2. Experimental Configuration

Polar mesosphere summer echoes heating experiments were carried out by European Incoherent SCATter (EISCAT) heating equipment located near Tromsø (69°35 N, 19°14 E) in northern Norway. The data were detected simultaneously by the EISCAT VHF radar and UHF radar, which were operating at relatively high but well-separated frequencies (224 and 930 MHz). Details of the heating facility used in the experiment are presented in Table 1.

The maximum of the apparent electron density between 80 and 90 km was used as a proxy for the strongest PMSEs. The electron density satisfying the threshold ($N_e \geq 3 \times 10^{10}$ m^{-3}) at an altitude of 91 km was used as a proxy for EPP (Rauf et al., 2019). It was helpful to observe the relationship between volume reflectivity and radar frequency of PMSEs during EPP events.

3. Observations of the VHF and UHF PMSEs with the Artificial Electron Heating Experiment

On 12 July 2007, the EISCAT VHF radar and UHF radar were operated simultaneously during the daytime in a special experiment to study the spectral characteristics of PMSEs. The experiment was carried out from 8:00 to 11:00 universal time (UT), but only the observations corresponding to the time interval from 9:00 to 10:00 UT were used, which corresponds to the study in Section 4. Figures 1 and 2 show the PMSEs observations that were carried out simultaneously with EISCAT VHF radar and UHF radar from 09:00 to 10:00 UT on 12 July 2007. From these figures, it is clear that PMSEs were rare and discontinuous when observed by EISCAT UHF radar, and the PMSEs height distribution ranged from 82 to 83 km. In contrast, PMSEs occurred more frequently and more clearly when observed by EISCAT VHF radar, and the height distribution ranged from 82 to 88 km.

Figure 2 shows that the UHF PMSEs corresponds to strong precipitation, and the region where EPP occurs partially overlaps the region where the PMSEs were observed by VHF radar. In fact, EPP also occurs at the same time the PMSEs were observed by VHF radar. Furthermore, Figure 1 shows almost no change in PMSEs intensity during the ionospheric artificial heating experiments, and PMSEs events are hardly affected by HF electromagnetic waves. The limited effect on PMSEs is due to the presence of EPP because the electron density in the mesosphere increases in the presence of EPP. Obvious absorption events will occur when the strong electromagnetic waves generated by the HF transmitter are vertically incident to the ionosphere, and the electromagnetic wave energy will attenuate rapidly, at which point it cannot reach the PMSEs region. Therefore, most of the heater wave energy was absorbed below the PMSEs layer, and this had little heating effect on the PMSEs (Rauf et al., 2018; Ullah et al., 2018).

4. Relationship Between the PMSEs Volume Reflectivity and Radar Frequency

4.1 Literature Database Analysis

In recent years, many radar observations have sought to verify the dependence of the echo intensity on frequency, although these observations have not reached the desired conclusion. Directly

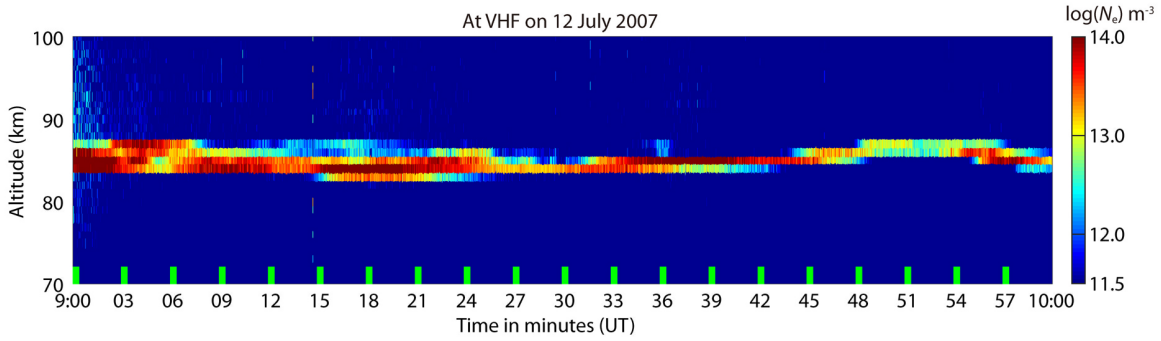

Figure 1. Polar mesosphere summer echoes (PMSEs) observed by EISCAT very high frequency (VHF) radar from 09:00 to 10:00 universal time (UT) on 12 July 2007. The vertical green rectangles represent the periods when radio waves were turned on during each heating cycle.

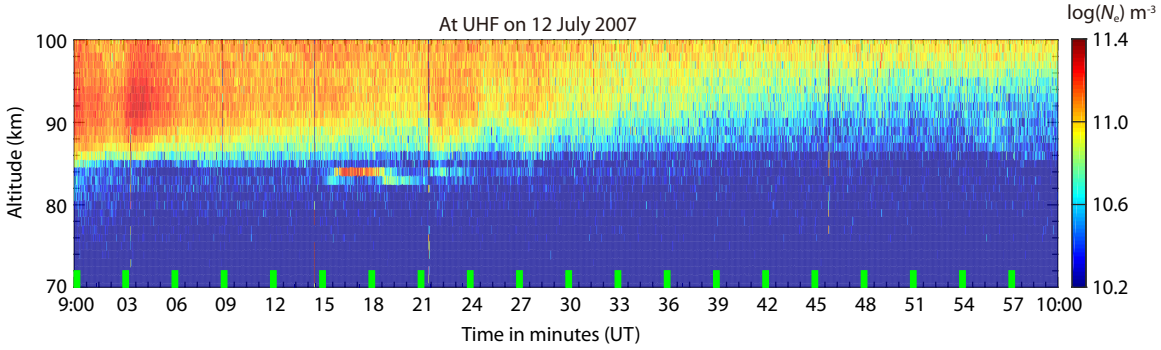

Figure 2. The same as Figure 1 but for the EISCAT ultra high frequency (UHF) radar.

analyzing the data results detected by radar of different frequencies is almost impossible because many observations are displayed in the form of the relative signal-to-noise ratio rather than as the absolute signal strength. The power being returned to the radar from a target has previously been referred to as reflectivity, which is a measure of the efficiency of a target at intercepting and returning radio frequency energy. The volume reflectivity is general radar terminology for the backscattering cross section per unit volume in the radar beam. The volume reflectivity is well known to be an independent parameter of the system, and it can be used to study the frequency dependence.

In this section, we mainly discuss the relationship between volume reflectivity and radar VHF and UHF bandwidth frequencies. Table 2 shows the volume reflectivity observed at different radar frequencies and in different locations. As shown in Table 2, the volume reflectivity clearly decreases with increasing radar frequency.

The scatter and fitting results for the volume reflectivity at different frequencies is given in Figure 3 based on the data in Table 2. The fitting expression is as follows:

$$\log_{10}(\eta) = 16.57 - 3.88\log_{10}(f), \quad (1)$$

where η is the volume reflectivity and f is the radar frequency. The volume reflectivity was found to be inversely proportional to the fourth power of frequency through this formula. That is, the scattering cross section per unit volume is inversely proportional to the fourth power of frequency.

4.2 Experimental Data Analysis

The relationship between volume reflectivity and radar frequency was verified experimentally. The original data dump provided by the EISCAT experiments were autocorrelation functions. These observations were routinely analyzed off-line in terms of electron number densities (or "apparent" electron densities, particularly for the PMSE region) by using the well-documented Grand Unified Incoherent Scatter Design and Analysis Package (GUISDAP; Lehtinen and Huuskonen, 1996). The apparent electron density was then converted to volume reflectivity by using the following equation:

$$\eta = \sigma_0 \times N_e, \quad (2)$$

where $\sigma_0 = 4.99 \times 10^{-29}$ m^{-2} is the effective scattering cross section of each electron and N_e is the apparent electron density (Röttger and La Hoz, 1990).

From Figure 2, we know the PMSEs intensity did not change significantly because EPP occurred during the artificial electron heating experiments. With the GUISDAP software package, the simultaneous observation data of the EISCAT VHF radar and UHF radar were analyzed with a 20 s integration time. This included the electron density corrected for height, which can represent the echo intensity. Figure 4 shows the variation profile of the corresponding radar echo with altitude observed by EISCAT radar. From 09:16 to 09:24 UT, 25 height profiles of VHF and UHF backscatter were recorded. We normalized the maximum values of the radar echoes in the VHF (solid blue lines) and UHF (dashed black lines) bands from 80 to 90 km. The start time corresponding to each figure is marked in Figure 4.

Table 2. Volume reflectivity observed with different types of radar.

Frequency (MHz)	Location	Reference	Reflectivity (m^{-1})
49.6	Tromsø (69°N)	Röttger et al. (1990)	2.0×10^{-12}
50.0	Poker Flat (65°N)	Kelley and Ulwick (1988)	9.0×10^{-15}
51.5	Resolute Bay (75°N)	Swarnalingam et al. (2011)	5.8×10^{-12}–4.2×10^{-16}
53.5	Andøya (69°N)	Havnes et al. (2001)	4.0×10^{-12}
53.5	Andøya (69°N)	Belova et al. (2007)	4.0×10^{-13}
53.5	Andøya (69°N)	Czechowsky et al. (1989)	1.9×10^{-9}–2.2×10^{-16}
53.5	Svalbard (78°N)	Röttger (2001)	2.2×10^{-14}–1.8×10^{-15}
55	Davis (69°S)	Morris et al. (2006)	3.7×10^{-11}–1.5×10^{-17}
224	Tromsø (69°N)	Röttger et al. (1990)	1.5×10^{-16}
224	Tromsø (69°N)	Hocking and Röttger (1997)	1.3×10^{-17}–1.3×10^{-15}
224	Tromsø (69°N)	Hoppe et al. (1988)	3.5×10^{-18}
224	Tromsø (69°N)	Belova et al. (2007)	1.5×10^{-14}
224	Tromsø (69°N)	Collis and Röttger (1990)	5.0×10^{-14}
450	Poker Flat (65°N)	Nicolls et al. (2007)	2.0–3.0×10^{-14}
500	Svalbard (78°N)	Röttger (2001)	5.3×10^{-19}–3.3×10^{-20}
930	Tromsø (69°N)	Röttger et al. (1990)	1.2×10^{-18}
930	Tromsø (69°N)	Belova et al. (2007)	1.5×10^{-18}
930	Tromsø (69°N)	Nicolls et al. (2007)	2.0×10^{-18}
1,290	Sondrestrom (67°N)	Cho et al. (1992)	2.5×10^{-18}

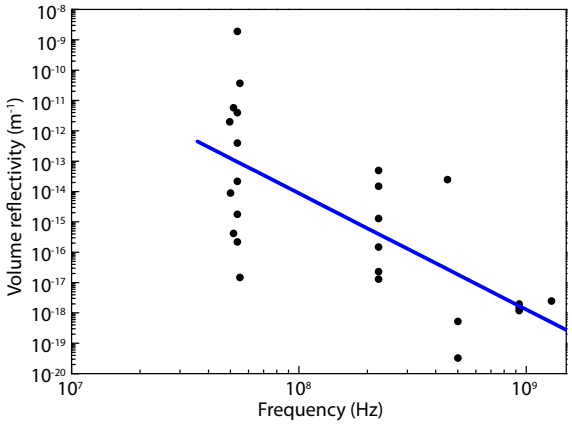

Figure 3. Relationship between volume reflectivity and radar frequency.

As shown in Figure 4, the heights of the strongest echoes observed by both VHF radar and UHF radar from 09:16:00 to 09:18:20 UT were clearly about 83.5 km. Moreover, the strongest radar echo in the UHF band gradually weakened after 09:18:40 UT, and the height of the strongest PMSE in the VHF and UHF bands gradually became inconsistent after 09:18:40 UT. In general, the strongest PMSE observed by VHF radar occurred at a higher altitude than that observed by UHF radar, except at 9:21:20 UT.

Because the PMSEs were observed simultaneously in the VHF and UHF bands, none was affected by strong electromagnetic waves. To further analyze the dependence between volume reflectivity and radar frequency, we calculated the volume reflectivity in the VHF and UHF bands, as shown in Figure 5. Figure 5 illustrates the maximum values of the volume reflectivity for the corresponding time intervals shown in Figure 4. The horizontal axis represents the observation time, and the vertical axis represents the logarithm of the radar volume reflectivity in the VHF and UHF bands. As shown in Figure 5, the maximum value of volume reflectivity in the UHF band was found to be fluctuant between 10^{-18} and 10^{-17} m^{-1}, whereas it was 10^{-15} to 10^{-14} m^{-1} in the VHF band.

From Figure 5, it is obvious that the η values at both the VHF and UHF bands were not stable and showed great variation. To analyze the radar frequency index at each height, we used the following formula:

$$n = \frac{\log_{10}(\eta_{\mathrm{VHF}}) - \log_{10}(\eta_{\mathrm{UHF}})}{\log_{10}(f_{\mathrm{VHF}}) - \log_{10}(f_{\mathrm{UHF}})}, \tag{3}$$

where n is the index of the wavenumber, η_{VHF} and η_{UHF} represent the volume reflectivity values corresponding to the VHF and UHF bands, and f_{VHF} and f_{UHF} represent the frequencies of VHF radar and UHF radar, respectively. Equation (3) is a simplified formula based on the volume reflectivity equation of Rapp and Lübken (2004) that was used to find the frequency index.

From Equation (3) and Figure 6, we obtained the ratio between −5.4 and −4.4, which fluctuated around −4.5 from 09:16:00 to 09:18:20 UT. In the region of the UHF band where the PMSEs were weak, the ratio was high, about −5, and it was basically consistent with the above-mentioned literature database analysis. For the in-

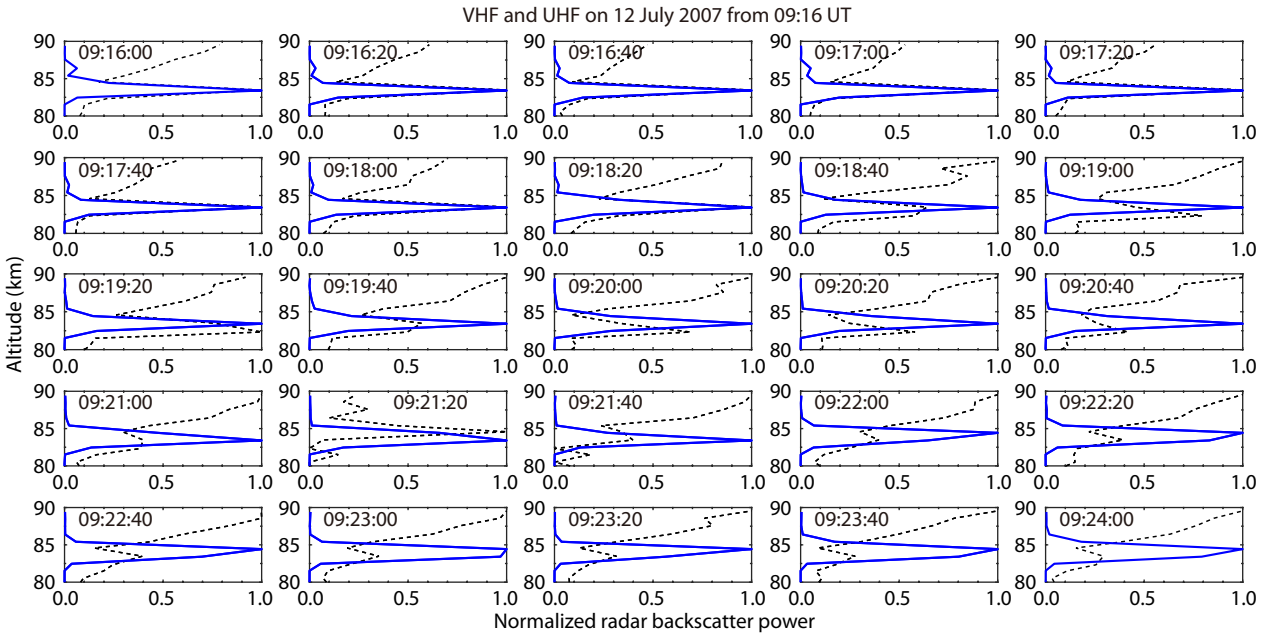

Figure 4. Normalized backscattered power spectra from the EISCAT VHF (solid blue lines) and UHF radar (dashed black lines) versus altitude. The backscatter height profiles were scaled by setting the maximum value of the strongest echo in each PMSEs profile to one.

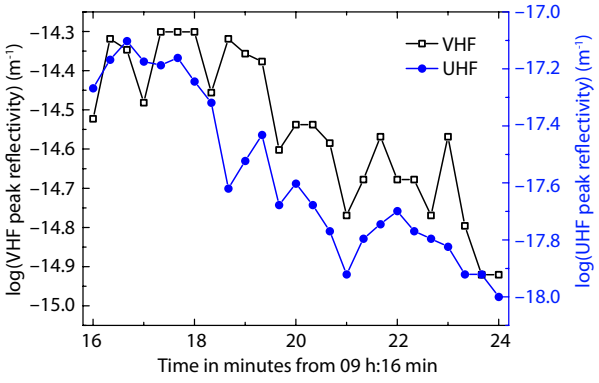

Figure 5. Maximum value of volume reflectivity versus time observed by VHF radar and UHF radar.

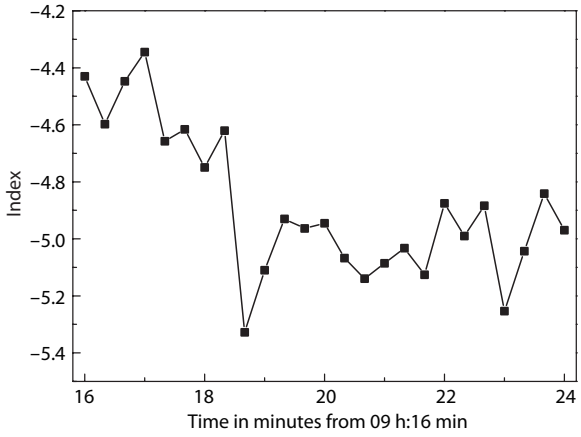

Figure 6. Indices based on Equation (3) and the corresponding data shown in Figure 5.

creasing frequency or the Bragg wavenumber, the volume reflectivity was found to decrease. A possible explanation is that the turbulence parameters were very different in the UHF and VHF EISCAT radar scattering volumes.

5. Discussion

It is well known that radar transmits an electromagnetic wave that is scattered at targets and is eventually received by a sensor. According to the definition, volume reflectivity depends on the ratio of the received to transmitted power when other radar parameters are determined. Furthermore, the volume reflectivity is proportional to the square of the reflection coefficient. Here, based on the theory of layered media, the altitude range from 83 to 88.4 km was divided evenly. Because permittivity has different values at different altitudes, if the range is divided into a different number of layers, the effect on the radar echoes will change. The reflection coefficients with the experimental data were calculated on each layer at the mesopause to determine the relationship between reflectivity and radar frequency. For the detailed model, please refer to Li HL et al. (2010). The squares of the reflection coefficients were calculated at altitudes from 83.0 to 88.4 km, and the results at each 0.9 km are given in Figure 7. The slope consistency at different heights is obvious at about 224 MHz. Table 3 shows the slopes and intercepts at different heights from Figure 7. Using a linearization analysis, we found that the logarithm of the reflection coefficients is proportional to the logarithm of the frequency.

The preceding analysis is based on the reflection coefficients with frequency changes at different altitudes. Although the trend is approximately similar, slight differences still exist between each layer. To eliminate these differences, the squares of the reflection coefficients were averaged across the range of 83.0 to 88.4 km. Figure 8 shows the relationship between the averaged squares of the reflection coefficients and the frequencies. The slope was

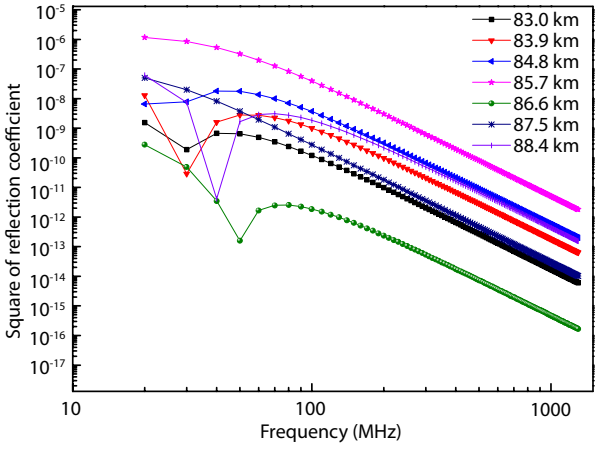

Figure 7. Square of the reflection coefficients versus frequencies for different altitudes.

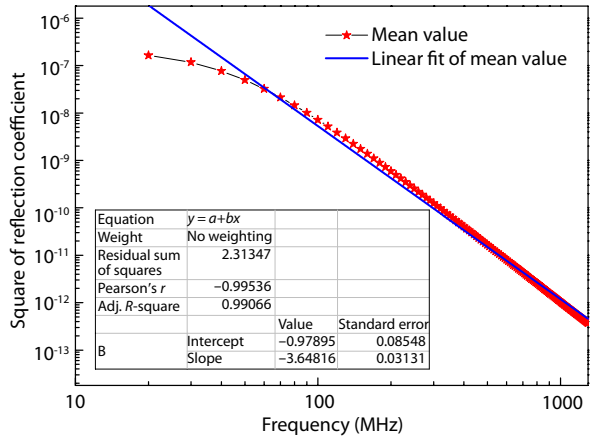

Figure 8. Mean squares of the reflection coefficients versus frequencies.

−3.65, and it conforms with the results in Table 3. Hence, the square of the reflection coefficient is inversely proportional to the fourth power of frequency. The volume reflectance is thus inversely proportional to the fourth power of frequency because of the proportionality between the volume reflectivity and the square of the reflection coefficient. Varney et al. (2011) showed that the variability in PMSEs reflectivity is related to the ice particle density, its height gradient, wave-induced disturbances, and the turbulent energy dissipation rate. Charged dust particles in the neutral atmosphere accumulate in irregular spatial distribution patterns. Satisfying the electroneutrality condition, the distribution of charged dust particles induces electron density variation, and that in turn changes the refraction index, which causes the radar echoes. The frequency dependence on PMSEs can probably be explained by electron density gradient theory, by which charged ice or dust particles are generated. Much more in-depth work is definitely needed with richer and more diverse learning content to further validate, refine, and extend these scientific findings.

6. Conclusions

In this study, we carried out PMSEs heating experiments of simultaneously observed by EISCAT 224 and 930 MHz radar on 12 July 2007. Combined with the updated results on volume reflectivity, the relationship between volume reflectivity and frequency was confirmed. Our results showed agreement between the theoretical and statistical results. We concluded the following:

(1) The probability of the PMSEs occurring at VHF is much higher than that at UHF, and the altitude of the PMSEs maximum observed by VHF radar is higher than the altitude of the PMSEs maximum observed by UHF radar.

(2) Overlapping regions were found between EPP and the PMSEs observed by VHF radar. Furthermore, HF heating has a limited effect on the PMSEs intensity when the UHF electron density is increased because of the presence of EPP.

(3) The volume reflectivity is inversely proportional to the fourth power of radar frequency, and a new qualitative analysis model is presented to verify the relationship between the volume reflectivity and frequency by analyzing the character of the irregularity. Results of the theoretical analysis are consistent with the experimental results. The volume reflectivity decreases rapidly with an increase in frequency.

Table 3. Slopes and intercepts at different heights.

Height (km)	Intercept	Slope
83.0	−3.05	−3.55
83.9	−2.73	−3.30
84.8	−1.78	−3.46
85.7	−0.10	−3.72
86.6	−5.15	−3.36
87.5	−1.78	−3.91
88.4	−2.69	−3.18

Acknowledgements

We are grateful to the EISCAT Scientific Association for providing the PMSE experimental data (http://portal.eiscat.se/schedule/schedule.cgi). The EISCAT Scientific Association is supported by China (China Research Institute of Radio Wave Propagation), Finland (Suomen Akatemia of Finland), Japan (the National Institute of Polar Research of Japan and Institute for Space–Earth Environmental Research at Nagoya University), Norway (Norges Forskningsråd of Norway), Sweden (the Swedish Research Council), and the UK (the Natural Environment Research Council). We also acknowledge the China Scholarship Council.

This research was funded by the Sichuan Science and Technology Program (no. 2019YJ0188), the National Natural Science Foundation of China (nos. 61671116, 61771096, 11905026), the National Key Research and Development Program of China (no. 2019YFA0210202), and Fundamental Research Funds for the Central Universities (nos. ZYGX2019Z006, ZYGX2019J012).

References

Belova, E., Dalin, P., and Kirkwood, S. (2007). Polar mesosphere summer echoes: a comparison of simultaneous observations at three wavelengths. *Ann.*

Geophys., *25*(12), 2487–2496. https://doi.org/10.5194/angeo-25-2487-2007

Blagoveshchenskaya, N. F., Borisova, T. D., Yeoman, T. K., Häggström, I., and Kalishin, A. S. (2015). Modification of the high latitude ionosphere F region by X-mode powerful HF radio waves: Experimental results from multi-instrument diagnostics. *J. Atmos. Solar Terr. Phys.*, *135*, 50–63. https://doi.org/10.1016/j.jastp.2015.10.009

Cai, H. T., and Ma, S. Y. (2007). Initial study of inversion method for estimating energy spectra of auroral precipitating particles from ground-based is radar observations. *Chin. J. Geophys.*, *50*(1), 12–21. https://doi.org/10.1002/cjg2.1005

Chen, C., and Scales, W. A. (2005). Electron temperature enhancement effects on plasma irregularities associated with charged dust in the Earth's mesosphere. *J. Geophys. Res.: Space Phys.*, *110*(A12), A12313. https://doi.org/10.1029/2005JA011341

Chilson, P. B., Belova, E., Rietveld, M. T., Kirkwood, S., and Hoppe, U. P. (2000). First artificially induced modulation of PMSE using the EISCAT heating facility. *Geophys. Res. Lett.*, *27*(23), 3801–3804. https://doi.org/10.1029/2000GL011897

Cho, J. Y. N., Kelley, M. C., and Heinselman, C. J. (1992). Enhancement of Thomson scatter by charged aerosols in the polar mesosphere: Measurements with a 1.29-GHz radar. *Geophys. Res. Lett.*, *19*(11), 1097–1100. https://doi.org/10.1029/92GL01155

Cho, J. Y. N., and Kelley, M. C. (1993). Polar mesosphere summer radar echoes: Observations and current theories. *Rev. Geophys.*, *31*(3), 243–265. https://doi.org/10.1029/93RG01535

Collis, P. N., and Röttger, J. (1990). Mesospheric studies using the EISCAT UHF and VHF radars: a review of principles and experimental results. *J. Atmos. Terr. Phys.*, *52*(6-8), 569–584. https://doi.org/10.1016/0021-9169(90)90054-Q

Czechowsky, P., Rüster, R., and Schmidt, G. (1979). Variations of mesospheric structures in different seasons. *Geophys. Res. Lett.*, *6*(6), 459–462. https://doi.org/10.1029/GL006i006p00459

Czechowsky, P., Reid, I. M., Rüster, R., and Schmidt, G. (1989). VHF radar echoes observed in the summer and winter polar mesosphere over Andøya, Norway. *J. Geophysi. Res.: Atmos.*, *94*(D4), 5199–5217. https://doi.org/10.1029/JD094iD04p05199

Ecklund, W. L., and Balsley, B. B. (1981). Long-term observations of the Arctic mesosphere with the MST radar at Poker Flat, Alaska. *J. Geophys. Res.: Space Phys.*, *86*(A9), 7775–7780. https://doi.org/10.1029/JA086iA09p07775

Havnes, O., Brattli, A., Aslaksen, T., Singer, W., Latteck, R., Blix, T., Thrane, E., and Trøim, J. (2001). First common volume observations of layered plasma structures and polar mesospheric summer echoes by rocket and radar. *Geophys. Res. Lett.*, *28*(8), 1419–1422. https://doi.org/10.1029/2000GL012420

Havnes, O., La Hoz, C., Næsheim, L. I., and Rietveld, M. T. (2003). First observations of the PMSE overshoot effect and its use for investigating the conditions in the summer mesosphere. *Geophys. Res. Lett.*, *30*(23), 2229. https://doi.org/10.1029/2003GL018429

Havnes, O., Kassa, M., and La Hoz, C. (2007). Time evolution of artificial electron heating in polar mesosphere summer echo layers. *J. Geophysi. Res.: Atmos.*, *112*(D8), D08202. https://doi.org/10.1029/2006JD007660

Havnes, O., Pinedo, H., La Hoz, C., Senior, A., Hartquist, T. W., Rietveld, M. T., and Kosch, M. J. (2015). A comparison of overshoot modelling with observations of polar mesospheric summer echoes at radar frequencies of 56 and 224 MHz. *Ann. Geophys.*, *33*(6), 737–747. https://doi.org/10.5194/angeo-33-737-2015

Hocking, W., and Röttger, J. (1997). Studies of polar mesosphere summer echoes over EISCAT using calibrated signal strengths and statistical parameters. *Rad. Sci.*, *32*(4), 1425–1444. https://doi.org/10.1029/97RS00716

Hoppe, U. P., Hall, C., and Röttger, J. (1988). First observations of summer polar mesospheric backscatter with a 224 MHz radar. *Geophys. Res. Lett.*, *15*(1), 28–31. https://doi.org/10.1029/GL015i001p00028

Kassa, M., Havnes, O., and Belova, E. (2005). The effect of electron bite-outs on artificial electron heating and the PMSE overshoot. *Ann. Geophys.*, *23*(12), 3633–3643. https://doi.org/10.5194/angeo-23-3633-2005

Kelley, M. C., and Ulwick, J. C. (1988). Large- and small-scale organization of electrons in the high-latitude mesosphere: Implications of the STATE data. *J. Geophysi. Res.: Atmos.*, *93*(D6), 7001–7008. https://doi.org/10.1029/JD093iD06p07001

La Hoz, C., Havnes, O., Næsheim, L. I., and Hysell, D. L. (2006). Observations and theories of Polar Mesospheric Summer Echoes at a Bragg wavelength of 16 cm. *J. Geophysi. Res.: Atmos.*, *111*(D4), D04203. https://doi.org/10.1029/2005JD006044

La Hoz, C., and Havnes, O. (2008). Artificial modification of polar mesospheric winter echoes with an RF heater: Do charged dust particles play an active role?. *J. Geophys. Res.: Atmos.*, *113*(D19), D19205. https://doi.org/10.1029/2008JD010460

Lehtinen, M. S., and Huuskonen, A. (1996). General incoherent scatter analysis and GUISDAP. *J. Atmos. Terr. Phys.*, *58*(1-4), 435–452. https://doi.org/10.1016/0021-9169(95)00047-X

Li, H. L., Wu, J., Huang, J. Y., and Wang, M. Y. (2010). Reflection characteristics of layered media in polar mesopause related to polar mesosphere summer echoes. *Plasma Sci. Technol.*, *12*(4), 416–420. https://doi.org/10.1088/1009-0630/12/4/07

Mahmoudian, A., Scales, W. A., Kosch, M. J., Senior, A., and Rietveld, M. (2011). Dusty space plasma diagnosis using temporal behavior of polar mesospheric summer echoes during active modification. *Ann. Geophys.*, *29*(11), 2169–2179. https://doi.org/10.5194/angeo-29-2169-2011

Mishin, E., Watkins, B., Lehtinen, N., Eliasson, B., Pedersen, T., and Grach, S. (2016). Artificial ionospheric layers driven by high-frequency radiowaves: An assessment. *J. Geophys. Res.: Space Phys.*, *121*(4), 3497–3524. https://doi.org/10.1002/2015JA021823

Morris, R. J., Murphy, D. J., Vincent, R. A., Holdsworth, D. A., Klekociuk, A. R., and Reid, I. M. (2006). Characteristics of the wind, temperature and PMSE field above Davis, Antarctica. *J. Atmos. Solar Terr. Phys.*, *68*(3-5), 418–435. https://doi.org/10.1016/j.jastp.2005.04.011

Nicolls, M. J., Heinselman, C. J., Hope, E. A., Ranjan, S., Kelley, M. C., and Kelly, J. D. (2007). Imaging of polar mesosphere summer echoes with the 450 MHz poker flat advanced modular incoherent scatter radar. *Geophys. Res. Lett.*, *34*(20), L20102. https://doi.org/10.1029/2007GL031476

Rapp, M., and Lübken, F. J. (2004). Polar mesosphere summer echoes (PMSE): Review of observations and current understanding. *Atmos. Chem. Phys.*, *4*(11-12), 2601–2633. https://doi.org/10.5194/acp-4-2601-2004

Rauf, A., Li, H. L., Ullah, S., Meng, L., Wang, B., and Wang, M. Y. (2018). Statistical study about the influence of particle precipitation on mesosphere summer echoes in polar latitudes during July 2013. *Earth Planets Space*, *70*, 108. https://doi.org/10.1186/s40623-018-0885-6

Rauf, A., Li, H. L., Ullah, S., Meng, L., Wang, B., and Wang, M. Y. (2019). Investigation of PMSE dependence on high energy particle precipitation during their simultaneous occurrence. *Adv. Space Res.*, *63*(1), 309–316. https://doi.org/10.1016/j.asr.2018.09.007

Reid, I. M., Czechowsky, P., Rüster, R., and Schmidt, G. (1989). First VHF radar measurements of mesopause summer echoes at mid-latitudes. *Geophys. Res. Lett.*, *16*(2), 135–138. https://doi.org/10.1029/GL016i002p00135

Reid, I. M., Rüster, R., Czechowsky, P., and Schmidt, G. (1988). VHF radar measurements of momentum flux in the summer polar mesosphere over Andenes (69°N, 16°E): Norway. *Geophys. Res. Lett.*, *15*(11), 1263–1266. https://doi.org/10.1029/GL015i011p01263

Röttger, J., Rietveld, M. T., La Hoz, C., Hall, T., Kelley, M. C., and Swartz, W. E. (1990). Polar mesosphere summer echoes observed with the EISCAT 933-MHz radar and the CUPRI 46.9-MHz radar, their similarity to 224-MHz radar echoes, and their relation to turbulence and electron density profiles. *Radio Sci.*, *25*(4), 671–687. https://doi.org/10.1029/RS025i004p00671

Röttger, J., and La Hoz, C. (1990). Characteristics of polar mesosphere summer echoes (PMSE) observed with the EISCAT 224 MHz radar and possible explanations of their origin. *J. Atmos. Terr. Phys.*, *52*(10-11), 893–906. https://doi.org/10.1016/0021-9169(90)90023-g

Röttger, J. (2001). Observations of the polar D-region and the mesosphere with the EISCAT Svalbard Radar and the SOUSY Svalbard Radar. *Mem. Natl. Inst. Polar Res.*, *54*, 9–20.

Scales, W. (2004). Electron temperature effects on small-scale plasma irregularities associated with charged dust in the Earth's mesosphere. *IEEE Trans. Plasma Sci.*, *32*(2), 724–730. https://doi.org/10.1109/TPS.2004.826082

Senior, A., Mahmoudian, A., Pinedo, H., La Hoz, C., Rietveld, M. T., Scales, W. A.,

and Kosch, M. J. (2014). First modulation of high-frequency polar mesospheric summer echoes by radio heating of the ionosphere. *Geophys. Res. Lett.*, *41*(15), 5347–5353. https://doi.org/10.1002/2014GL060703

Sinnhuber, M., Nieder, H., and Wieters, N. (2012). Energetic particle precipitation and the chemistry of the mesosphere/lower thermosphere. *Surv. Geophys.*, *33*(6), 1281–1334. https://doi.org/10.1007/s10712-012-9201-3

Swarnalingam, N., Hocking, W. K., and Drummond, J. R. (2011). Long-term aspect-sensitivity measurements of polar mesosphere summer echoes (PMSE) at Resolute Bay using a 51.5 MHz VHF radar. *J. Atmos. Solar Terr. Phys.*, *73*(9), 957–964. https://doi.org/10.1016/j.jastp.2010.09.032

Ullah, S., Li, H. L., Abdur, R., Meng, L., Wang, B., and Wang, M. Y. (2018). PMSE dependence on frequency observed simultaneously with VHF and UHF radars in the presence of precipitation. *Plasma Sci. Technol.*, *20*(11), 115302. https://doi.org/10.1088/2058-6272/aac8d4

Varney, R. H., Kelley, M. C., Nicolls, M. J., Heinselman, C. J., and Collins, R. L. (2011). The electron density dependence of polar mesospheric summer echoes. *J. Atmos. Solar Terr. Phys.*, *73*(14-15), 2153–2165. https://doi.org/10.1016/j.jastp.2010.07.020

Wang, X., Cannon, P., Zhou, C., Honary, F., Ni, B. B., and Zhao, Z. Y. (2016). A theoretical investigation on the parametric instability excited by X-mode polarized electromagnetic wave at Tromsø. *J. Geophys. Res. Space Phys.*, *121*(4), 3578–3591. https://doi.org/10.1002/2016JA022411

Yi, W., Reid, I. M., Xue, X. H., Younger, J. P., Murphy, D. J., Chen, T. D., and Dou, X. K. (2017a). Response of neutral mesospheric density to geomagnetic forcing. *Geophys. Res. Lett.*, *44*(16), 8647–8655. https://doi.org/10.1002/2017GL074813

Yi, W., Reid, I. M., Xue, X. H., Younger, J. P., Spargo, A. J., Murphy, D. J., Chen, T. D., and Dou, X. K. (2017b). First observation of mesosphere response to the solar wind high-speed streams. *J. Geophys. Res.: Space Phys.*, *122*(8), 9080–9088. https://doi.org/10.1002/2017JA024446

Yi, W., Reid, I. M., Xue, X. H., Murphy, D. J., Hall, C. M., Tsutsumi, M., Ning, B. Q., Li, G. Z., Younger, J. P., … Dou, X. K. (2018). High- and middle-latitude neutral mesospheric density response to geomagnetic storms. *Geophys. Res. Lett.*, *45*(1), 436–444. https://doi.org/10.1002/2017GL076282

Zhang, B. C., Liu, R. Y., and Liu, S. L. (2001). Simulation study of the influence of the precipitating electrons on the polar ionosphere. *Chin. J. Geophys.*, *44*(3), 302–311. https://doi.org/10.1002/cjg2.145

Zou, Z. C., Xue, X. H., Yi, W., Shen, C. L., Yang, C. Y., Tang, Y. H., Chen, T. D., and Dou, X. K. (2020). Response of the high-latitude upper mesosphere to energetic electron precipitation. *Astrophys. J.*, *893*(1), 55. https://doi.org/10.3847/1538-4357/ab7eb0